Proceedings of the Czech–Japanese Seminar in Applied Mathematics 2010
Czech Technical University in Prague, August 30 - September 4, 2010
pp. 11–17

# NUMERICAL SIMULATION OF STEADY TURBULENT FLOW

PETR FURMÁNEK[1], JIŘÍ FÜRST[2], KAREL KOZEL[2]

**Abstract.** The aim of this work is to summarise and compare the results of numerical simulations of steady transonic flows in 2D and 3D obtained by two modern finite volume schemes. Implemented schemes are the so called Modified Causon's scheme [15] (based on TVD form of MacCormack scheme) and WLSQR scheme [3] (WENO approach) combined with HLLC numerical flux. Chosen test cases are steady inviscid transonic flow over the NACA 0012 profile and steady turbulent transonic flow around the ONERA M6 wing. Turbulent effects are simulated using the Spalart-Allmaras and SST models (in 3D). Obtained numerical results are compared both in-between and with experimental data with very good agreement.

**Key words.** FVM, Spalart-Allmaras, SST, transonic flow, turbulent flow, TVD, WENO.

**AMS subject classifications.** 76M12, 76H05, 76N99

**1. Introduction.** With huge development of computational fluid dynamics methods in the late years, the turbulence models became a widely spread industrial standard. However, it is sometimes difficult to combine given turbulent model with given numerical scheme. It is therefore necessary to perform numerical tests to validate various combinations of schemes and turbulence models. The authors are testing several such combinations using modern high-order finite volume schemes and different turbulence models.

**2. Mathematical Model.** The governing system of equations is generally represented by the system of Navier-Stokes equations describing the motion of viscous compressible fluid, which can be written down in dimension-less vector form as

$$W_t + F_x + G_y + H_z = 0, \tag{2.1}$$

where

$$\begin{aligned}
F &= F^c - \frac{1}{Re}F^v,\ G = G^c - \frac{1}{Re}G^v,\ H = H^c - \frac{1}{Re}H^v \\
W &= (\rho, \rho u, \rho v, \rho w, e)^T \\
F^c &= (\rho u, \rho u^2 + p, \rho uv, \rho uw, (e+p)u)^T \\
G^c &= (\rho v, \rho uv, \rho v^2 + p, \rho vw, (e+p)v)^T \\
H^c &= (\rho w, \rho uv, \rho uw, \rho w^2 + p, (e+p)w)^T \\
F^v &= (0, \tau_{xx}, \tau_{xy}, \tau_{xz}, u\tau_{xx} + v\tau_{xy} + w\tau_{xz} + \frac{\kappa}{Pr}\lambda u_x)^T \\
G^v &= (0, \tau_{xy}, \tau_{yy}, \tau_{yz}, u\tau_{xy} + v\tau_{yy} + w\tau_{yz} + \frac{\kappa}{Pr}\lambda v_y)^T \\
H^v &= (0, \tau_{xz}, \tau_{yz}, \tau_{zz}, u\tau_{xz} + v\tau_{yz} + w\tau_{zz} + \frac{\kappa}{Pr}\lambda w_z)^T
\end{aligned}$$

$$p = (\kappa - 1)\big[e - \frac{1}{2}\rho(u^2 + v^2 + w^2)\big],\ \kappa = \frac{c_p}{c_v} \quad (\textit{equation of state}) \tag{2.2}$$

[1]VZLÚ a.s., Prague
[2]CTU in Prague, Faculty of Mechanical Engineering, Department of Technical Mathematics

and $W$ is the vector of conservative variables, $F^c, G^c, H^c$ are the inviscid fluxes, $F^v, G^v, H^v$ are the viscous fluxes, $\rho$ is the density; $(u, v, w)$ is the velocity vector; $p$ is the pressure; $e$ is the total energy per unit volume, $\tau$ is viscous stress tensor, $Re$ is the Reynolds number, $Pr$ is the Prandtl number, $\lambda$ is heat flux coefficient. System (2.1) was simplified in case of inviscid simulation by neglecting the viscous fluxes (i.e. used as the system of Euler equations) or modified in the case of turbulent flow by the Reynolds averaging (i.e. turned into RANS system).

**3. Numerical Methods.** Numerical solution of the governing system of equations was realized by the finite volume method, particularly by the following high-order schemes.

**3.1. Modified Causon's scheme (MCS).** *Modified Causon's scheme* [15] is based on classical explicit MacCormack predictor-corrector scheme in TVD form, which delivers very good results. However, it also entails disadvantageous demands on both computational memory and power. Therefore a simplification saving approximately 30% of computational time was proposed by Causon [6] by introducing a special type of artificial dissipation (AD). This new scheme was still TVD, but the influence of AD turned out to be too strong. The authors on the other hand proposed another modification based on Causon's scheme (referred to as the Modified Causon's scheme), which is not TVD, but keeps the advantages of the Causon's scheme while clearing out its drawbacks at the same time.

**3.2. Weighted Least-Square Reconstruction scheme (WLSQR).** When solving (2.1) with the WLSQR scheme [15], [3], the real inviscid fluxes in the surface integrals are approximated by numerical ones (in our case by the HLLC flux [7]). The high order accuracy in time is achieved in a standard way by using the interpolated values at the cell faces. The interpolation is obtained using the weighted least-square approach, which usually shows better convergence to steady state than the methods with Barth's limiter. Advancing in time is realized by the non-linear implicit dual-time backward Euler method. The resulting sparse system of linear equations is solved by GMRES with ILU(0) preconditioning. The dimension of the Krylov subspace is chosen between 10–40 and the maximum number of iteration is set to 10–50. If the steady solution is not found in prescribed number of iterations the computation proceeds in the next time step.

**4. Turbulence Models.** The chosen turbulence models are based on Boussinesq approximation [4], which is an analogy to Newtons friction law. As a consequence, the additional turbulent stresses are evaluated by augmenting the molecular viscosity with an eddy viscosity.

**4.1. Spalart-Allmaras model.** Using this model, the eddy viscosity is obtained as a solution of one transport equation for viscosity-like variable $\tilde{\nu}$. This model is commonly used for aerodynamical turbulence simulation and was calibrated to suit this purpose [8].

**4.2. SST $k-\omega$ model.** Menter's SST model [9] is a two equation eddy-viscosity model for turbulent kinetic energy $k$ and specific dissipation rate $\omega$. It uses standard $k-\omega$ formulation in the inner parts of the boundary layer and hence can be used as a Low-Re turbulence model without any extra damping functions. As the usual $k-\omega$ models are very sensitive to the inlet free-stream boundary conditions, the SST model switches to $k-\epsilon$ behaviour in free-stream to avoid this problem.

## 5. Numerical Results.

**5.1. 2D Steady Transonic Inviscid Flow.** A standard test case for two-dimensional steady flow was chosen to verify the MCS scheme - steady transonic inviscid flow over the NACA 0012 profile with inlet Mach number $M_\infty = 0.8$ and angle of attack $\alpha = 1.25°$. Steady computation of flow around the NACA 0012 aerofoil was carried out using structured FVM mesh made from quadrilaterals with 8400 computational cells (140 cells around the profile). The solution domain covered by the computational mesh was 20 profile chords long and 20 profile chords wide.

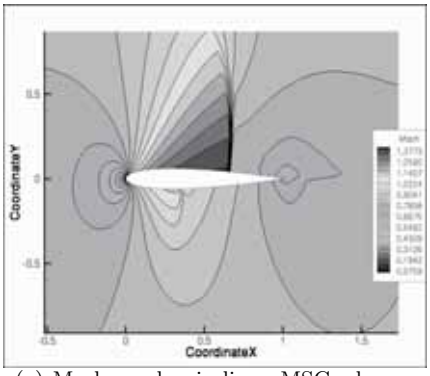


(a) Mach number isolines, MSC scheme.

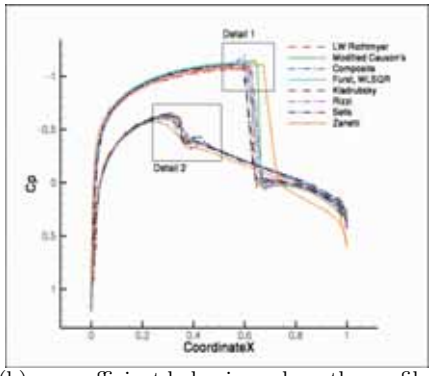


(b) $c_p$ coefficient behaviour along the profile, comparison of various schemes.

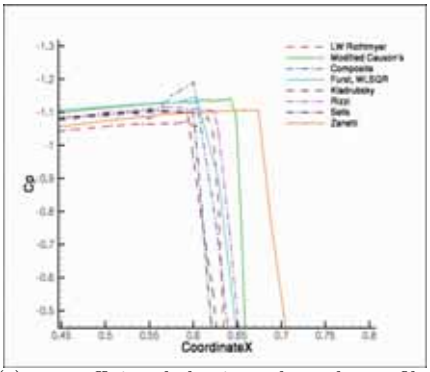


(c) $c_p$ coefficient behaviour along the profile, comparison of various schemes. Detail 1.

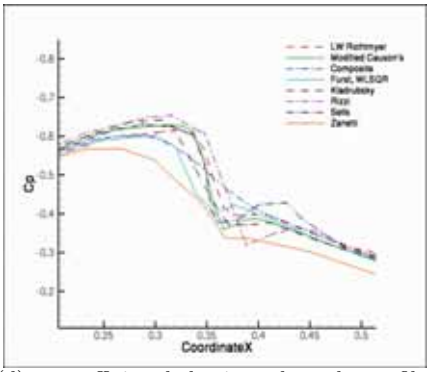


(d) $c_p$ coefficient behaviour along the profile, comparison of various schemes. Detail 2

FIG. 5.1. *Inviscid transonic flow over the NACA 0012 aerofoil,* $M_\infty = 0.8, \alpha = 1.25°$. *Comparison of various schemes.*

Figure 5.1 shows that the implemented scheme is in a good correspondence with the results of other authors ([12], [15], [13], [14]) and also with expectations about behaviour of the investigated flow regime. A closer look on regions in the proximity of the shock-wave shows that the MCS scheme does not produce spurious oscillations and captures both upper and lower margins of the shock-wave with very good precision (including the Zierep singularity on figure 5.1(d)).

**5.2. 3D Laminar Flow.** The MCS scheme was extended for 3D laminar flow and tested on subsonic flow around the ONERA M6 wing with inlet Mach number $M_\infty = 0.5$, the angle of attack $\alpha = 0°$ and the Reynolds number $\mathrm{Re} = 1 \times 10^6$. Obtained numerical results are only preliminary and unfortunately cannot be com-

pared with experimental results, but they show all the characteristics as expected. Unsteady flow develops near the trailing edge of the wing. Although this simulation has no physical meaning, it serves as a valuable test of the scheme's capabilities.

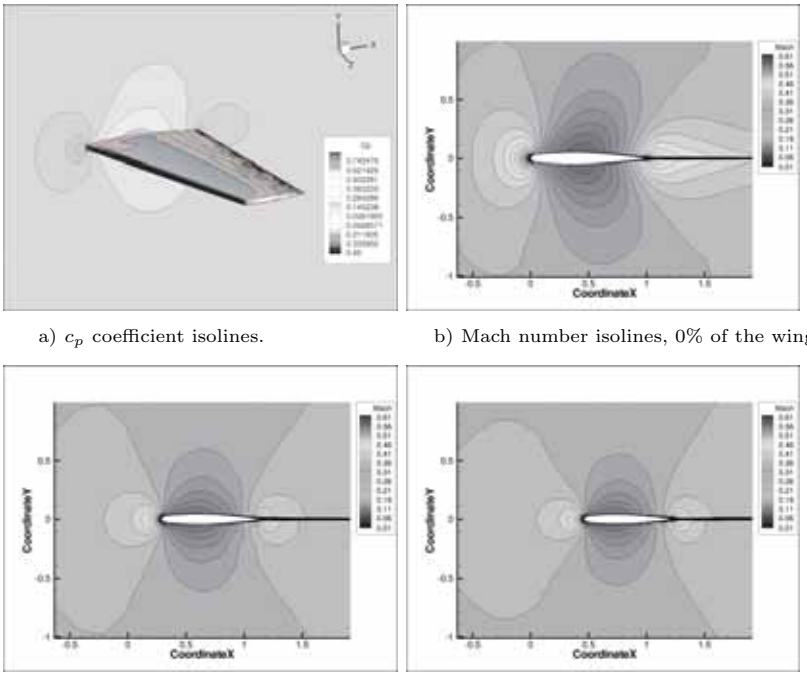


a) $c_p$ coefficient isolines.

b) Mach number isolines, 0% of the wing span.

c) Mach number isolines, 50% of the wing span.

d) Mach number isolines, 80% of the wing span.

FIG. 5.2. *Laminar subsonic flow over the ONERA M6 wing,* $M_\infty = 0.6, \alpha = 0°$. *Modified Causon's scheme.*

**5.3. 3D Steady Inviscid and Turbulent Flow.** Considering 3D turbulent computation, the schemes were tested on transonic flow over the ONERA M6 wing (which is another well-known test case [11]). The inlet Mach number was $M_\infty = 0.8395$, the angle of attack $\alpha = 3.06°$ and the Reynolds number $\mathrm{Re} = 11.72 \times 10^6$. Obtained numerical results show very good correspondence with experimental data (Figs. 5.3 and 5.4). The typical $\lambda$-shaped structure formed by the shock waves is clearly visible on the top side of the wing in both inviscid and turbulent case. The inviscid model predicts sharper and steeper shock waves and pushes them closer to the trailing edge of the wing, as expected. The turbulent models on the other hand correspond better to the real flow. The Spalart-Allmaras model seems to be a little more precise (at least for this case of flow). Considering efficiency of the mentioned schemes, the MCS is somewhat limited because of its ability to handle only structured meshes and also due to its current explicit form (the implicit version has already been implemented, but not yet tested for the case of 3D flow).

**6. Conclusion.** Considering the 2D steady inviscid regime, the MCS scheme delivers very good results. It is able to capture important characteristics of transonic flow, such as the position and intensity of the shock wave. In 3D case, a very good correspondence was achieved between the experimental and numerical results for both inviscid and viscous case. Chosen combinations of turbulence models and numerical

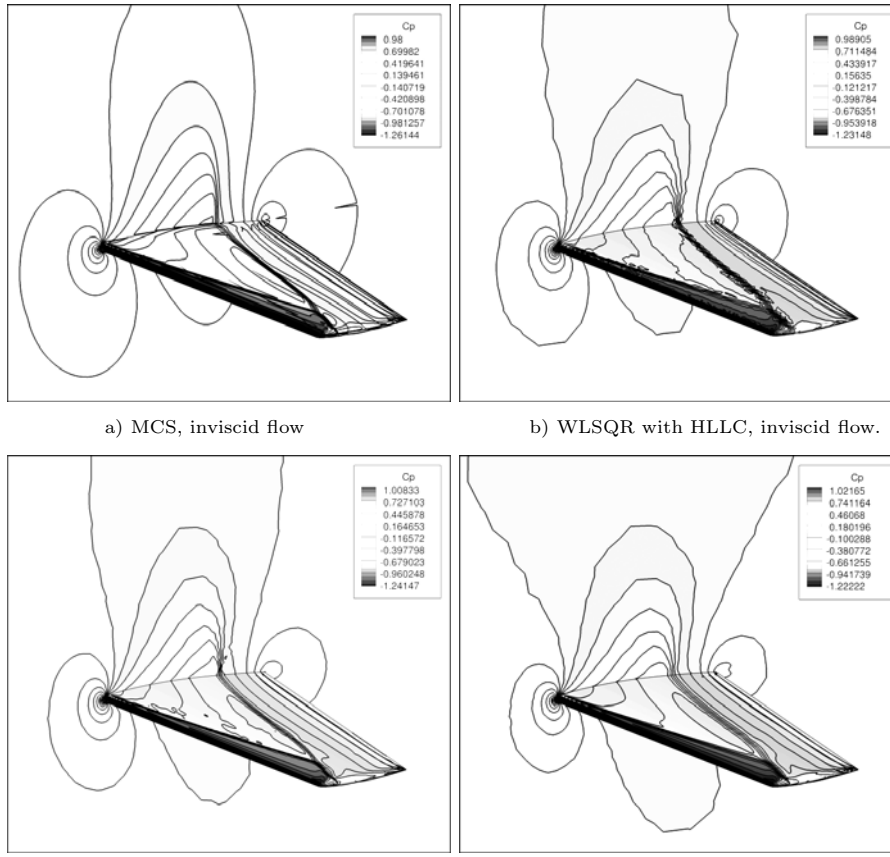


a) MCS, inviscid flow

b) WLSQR with HLLC, inviscid flow.

c) WLSQR with HLLC, Spalart-Allmaras.

d) WLSQR with HLLC, SST $k - \omega$.

FIG. 5.3. *$c_p$ coefficient isolines top side of the wing, comparison of inviscid and turbulent computation.*

scheme perform very well, the Spalart-Allmaras seems a bit better. Both models show very good usability for numerical simulations transonic flows without significant separation. Future steps intended are the implementation of another turbulence model for 2D unsteady flow and the implementation of unsteady turbulent effects.

**Acknowledgement.** This work was partly supported by Research Plans No. 6840770010 and MSM 0001066902 and grants GACR 201/08/0012 and P101/10/1329.

REFERENCES

[1] H.C CHENA, V.C PATELA AND S JUA. *Solutions of Reynolds-averaged Navier-Stokes equations for three-dimensional incompressible flows.* Journal of Computational Physics **88**, Issue 2 (1990), 305–336.

[2] J. DONEA. *An arbitrary Lagrangian-Eulerian finite element method for transient fluid-structure interactions.* Comput. Methods Apll. Mech. Eng. **33** (1982), 689–723.

[3] J. FÜRST. *A Weighted Least Square Scheme for Compressible Flows.* Flow, Turbulence and Combustion [online] **76** , no. 4 (2006), 331–342.

[4] J. BOUSSINESQ. *Théorie de l'écoulement tourbillonnant et tumultueux des liquides dans les lits rectilignes a grande section.* (vol.1). Gauthier-Villars (1897).

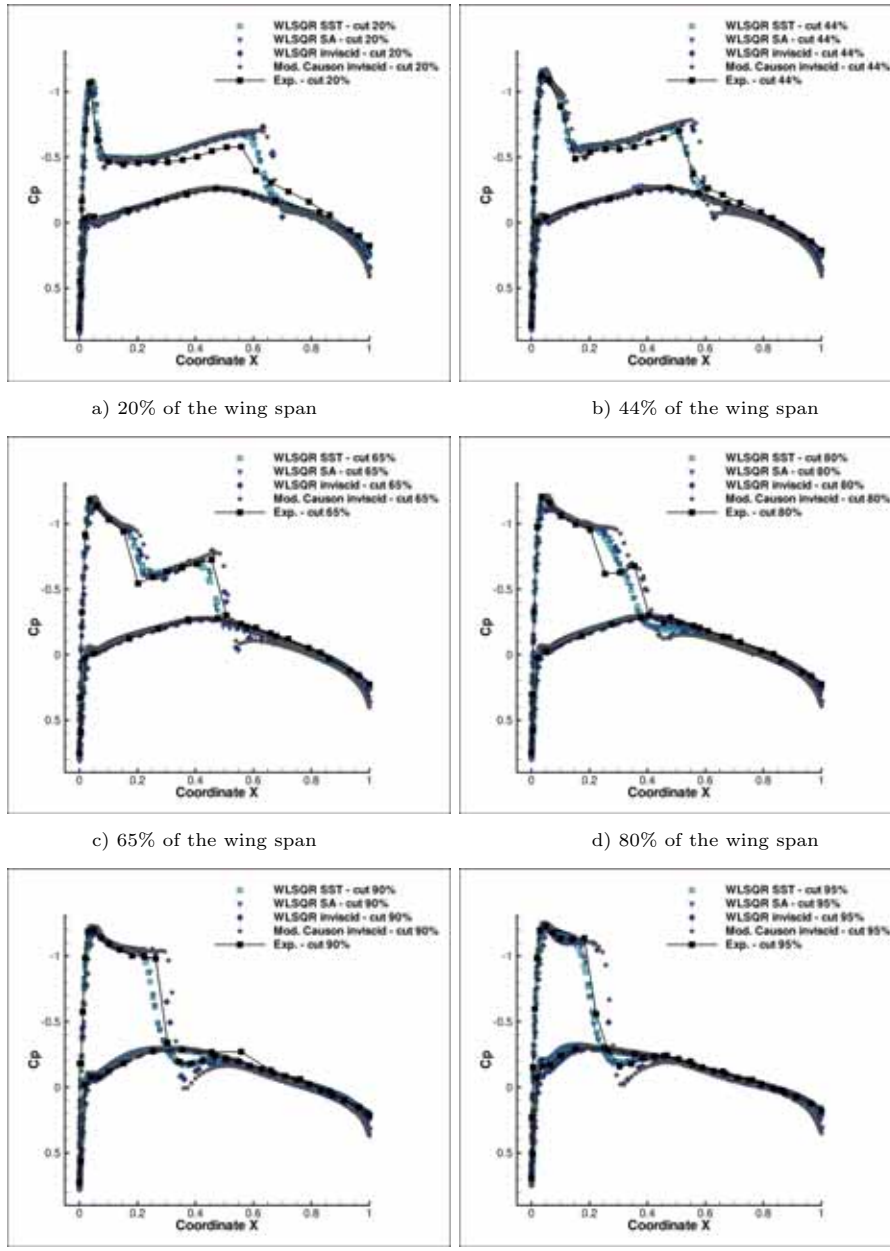


a) 20% of the wing span

b) 44% of the wing span

c) 65% of the wing span

d) 80% of the wing span

e) 90% of the wing span

f) 95% of the wing span

FIG. 5.4. *$c_p$ coefficient in the cuts alongside the wing, comparison of the experimental and numerical results.*

[5] P. Furmánek, J. Fürst, K. Kozel. *High Order Finite Volume Schemes for Numerical Solution of 2D and 3D Transonic Flows.* Kybernetika **45**, no. 4 (2009), 567–579.

[6] D. M. Causon. *High resolution fnite volume schemes and computational aerodynamics.* In: J. Ballmann and R. Jeltsch, eds., Nonlinear Hyperbolic Equations - Theory, Computation Methods and Applications, volume 24 of Notes on Numerical Fluid Mechanics, pages 63-74, Braunschweig, Vieweg (1989).

[7] P. Batten, M. A. Leschziner and U. C. Goldberg. *Average-State Jacobians and Implicit*

*Methods for Compressible Viscous and Turbulent Flows.* Journal of Computational Physics **137**, Issue 1 (1997) 38–78.

[8] P.R. Spalart and S.R. Allmaras. *A One-Equation Turbulence Model for Aerodynamic Flows.* AIAA Paper (1992), 92-0439.

[9] F.R. Menter. *Zonal Two Equation k-$\omega$ Turbulence Models for Aerodynamic Flows.* AIAA Paper (1993) 93-2906.

[10] D.C. Wilcox. *Re-assessment of the scale-determining equation for advanced turbulence models.* AIAA Journal **26** (1988), 1414–1421.

[11] V. Schmitt and F. Charpin. *Pressure Distributions on the ONERA-M6-Wing at Transonic Mach Numbers. Experimental Data Base for Computer Program Assessment.* Report of the Fluid Dynamics Panel Working Group 04, AGARD AR 138 (1979).

[12] G. McNamara and G. Zanetti. *Use of the Bolzmann Equation to Simulate Lattice-Gas Automata.* Phys. Rev. Lett. **61** (1988), 2332–2335.

[13] B. Müller and A. Rizzi. *Modelling of turbulent transonic flow around aerofoils and wings.* Communications in Applied Numerical Methods **6** (1990), 603–613. doi:10.1002/cnm.1630060805

[14] P. Furmánek, J. Dobeš, J. Fořt, J. Fürst, M. Kladrubský et al. *Numerical Solution of Transonic Flows over an Airfoil and a Wing.* In: CMFF'06 Conference Proceedings [CD-ROM]. Budapest: Budapest University of Technology and Economics (2006).

[15] J. Fürst. *Numerical Solution of Transonic Flow Using Modern Schemes of Finite volume Method and Finite Differences.* Dissertation thesis (in Czech), ČVUT, Praha (2001).